EEG Quality: Origin and Reduction of the EEG Cardiac-Related Artefact

8

Stefan Debener, Cornelia Kranczioch, and Ingmar Gutberlet

1 Introduction

With the advent of purpose-built "MR-compatible" EEG recording hardware, the simultaneous acquisition of EEG and fMRI has recently become more widespread (for reviews, see Herrmann and Debener 2007; Laufs et al. 2008). Nevertheless, the MRI scanner remains a hostile environment for EEG recordings, and ensuring good EEG signal quality can be a challenging task (e.g. Parkes et al. 2006). The level of EEG data quality that can be achieved from simultaneous recordings is a matter of ongoing investigation, but a common view is that a certain loss of quality is unavoidable and must be tolerated (Debener et al. 2007b). Nonetheless, combined EEG and fMRI data acquisitions in a single session are an attractive alternative to separate acquisitions in some circumstances, as discussed throughout this book (Babiloni et al. 2004; Debener et al. 2006; Horwitz and Poeppel 2002). The reduction of artefacts that contaminate the EEG signal as much as possible is necessary to make full use of the potential of EEG–fMRI.

The MRI environment is known to introduce several different types of EEG artefact, among them the gradient artefact and the cardiac pulse-related (often referred to as ballistocardiogram or BCG) artefact.[1] This chapter focuses on the pulse artefact: its origin, characteristics of it, and methods of reducing or eliminating it. After introducing the conceptual and statistical characteristics that define the pulse artefact, we discuss the mechanisms that give rise to the pulse artefact and present a two-factor pulse artefact model. We will review and compare different ways of removing it. We will focus on several recording

[1]In this work we use the term "pulse-related artefact" or "pulse artefact" to designate what many authors call the BCG. This choice reflects the editors' wish to use a term that can encompass all possible (not just ballistic) mechanisms that give rise to the EEG artefact (see Sect. 3).

Prof. Dr. Stefan Debener (✉)
Biomagnetic Center, Dept. of Neurology, University Hospital Jena, Erlanger Allee 101, D-07747 Jena, Germany
e-mail: stefan@debener.de

C. Mulert and L. Lemieux (eds.), *EEG–fMRI*
DOI: 10.1007/978-3-540-87919-0_8, © Springer Verlag Berlin Heidelberg 2010

and analysis details that have been barely acknowledged in the literature and can have a significant impact on the quality of the pulse artefact correction step, and thus on the final EEG data quality.

With amplitudes that can be several orders of magnitudes larger than the neuronal EEG signal, the MR image acquisition artefact is more prominent than the pulse artefact. However, the imaging artefact's perfect predictability and relative reproducibility (its amplitude and shape can be affected by subject motion) mean that it can be removed relatively easily from the EEG by postprocessing. Moreover, the impact of the gradient artefact could, in principle, be reduced by employing interleaved recording designs (see the chapter "Experimental Design and Data Analysis Strategies").

2 Characteristics of the Pulse Artefact

The pulse artefact is clearly visible on EEGs recorded inside the MR scanner even in the absence of scanning, and contributes amplitudes and frequencies that are close to the range of the usual EEG signal, with an amplitude that is on the order 50 μV (at 1.5 T) and has a resemblance to epileptic spikes. As will be discussed in the next section, the pulse artefact is a typical example of a mesogenous artefact, since it results from the interaction between the active cardiovascular system (endogenous contribution) and the main static (B_0) field inside the MRI scanner (exogenous contribution).[2]

Figure 1 shows a typical example of the pulse artefact and how it interferes with ongoing EEG signals recorded inside a 1.5 T MRI scanner. Its defining feature is synchrony with the cardiac rhythm captured on simultaneously recorded ECG. Careful comparison of the pulse artefact and ECG reveals a delay of approximately 200 ms between the R peak and the peak artefact in the EEG traces (Allen et al. 1998), indicating that the artefact is not simply a volume-conducted electrical ECG artefact, with fluctuations in the interartefact interval reflecting fluctuations in the subject's heart rate (and likely in other cardiovascular parameters). As can be seen, the artefact amplitude can be substantially larger than occipital EEG alpha oscillations. The peak amplitude can vary markedly across individuals, channels and MRI scanners. As a rule of thumb, EEG electrodes far from the EEG reference electrode express larger amplitudes, and a high-field MRI scanner causes larger amplitudes than a scanner with a lower field (Debener et al., 2008). In addition, the artefact's morphology can vary between EEG channels, and these channel-by-channel differences do not seem to be completely accounted for by scaling differences. The interchannel variability in artefact latency and morphology as well as in morphology over time (e.g. channel P7 in Fig. 1) is a key consideration for artefact reduction methods.

It is noteworthy that the spatial features of the pulse artefact have rarely (Allen et al. 1998; Nakamura et al. 2006) been investigated in detail (Debener et al., 2007). Figure 2

[2]The pulse artefact was originally described in clinical EEGs recorded outside the MRI and in the supine position, which can cause a pulsatile, rocking head rotation. Here we limit the pulse artefact to intra-MRI EEG recordings.

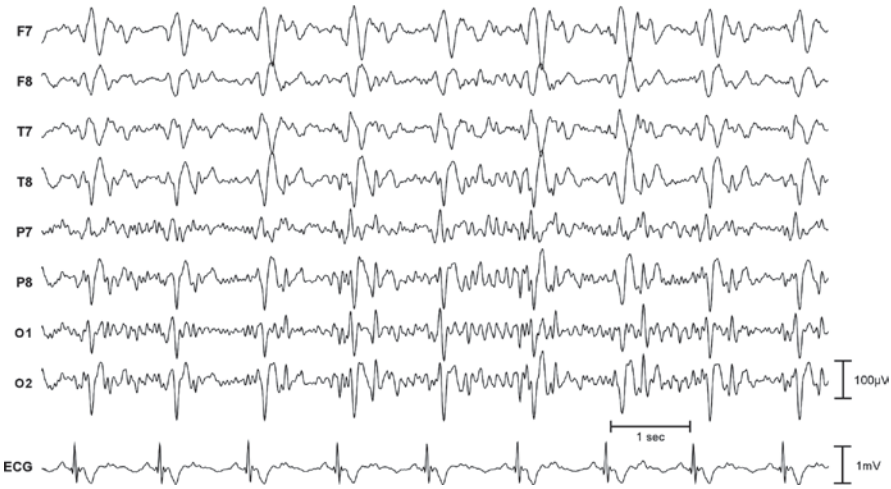

Fig. 1 Example of the pulse artefact in ongoing EEG data recorded in a 1.5 T MRI scanner without MRI scanning. EEG traces at lateral sites over the left and right hemispheres, where the artefact is usually most pronounced, are shown. Note the temporal pattern, which corresponds to the cardiac cycle and is delayed in relation to the R peak of the ECG (*bottom trace*) by about 200 ms. Also apparent are the different morphologies of the artefact at different scalp sites, and, across electrodes, the asymmetric and asynchronous patterns of activity. The ECG was recorded simultaneously from an electrode attached to the lower back and referenced to the EEG recording reference (Cz), a favourable ECG recording scheme. Exposure to a strong magnetic field distorts the ECG signal most during the ST interval, whereas the QRS interval is unchanged compared to outside MRI scanner recordings

illustrates the main spatial features of the pulse artefact, showing the time-domain averaged signal (the *evoked pulse artefact*) and topographies at some peak latencies. In order to obtain the evoked pulse artefact, the onset of each cardiac cycle was determined and used as a time-locking event (in this example, this was the Q wave in the ECG recording). The upper part of the figure shows the evoked artefact traces at all EEG electrodes together with the mean global field power (GFP). The GFP summarizes activity irrespective of the polarity of the potentials and corresponds to the spatial standard deviation across all recorded channels (Skrandies 1990). It can be seen that the pulse artefact starts approximately 150 ms after the Q peak and has two peaks at approximately 230 and 330 ms. Also, the pulse artefact lasts until at least ~500 ms after the ECG Q wave. Corresponding voltage maps at selected GFP peak latencies reveal some interesting features. First, in most cases the artefact topography can be characterised by a low spatial frequency. Therefore, the pulse artefact can be best characterised by more complete spatial coverage of the head sphere. Poor spatial coverage, for instance due to a focus on a few electrodes around the vertex (Nakamura et al. 2006) may miss important features of the artefact. Second, the topography changes substantially over time. Repeating patterns can be observed (for example, compare the maps at 176 and 464 ms in Fig. 2), although they are slightly rotated relative to each other. We have consistently observed this moving topographical pulse artefact pattern, irrespective of the number of EEG channels (30–62), the MRI scanner manufacturer (Siemens, Philips), the MRI

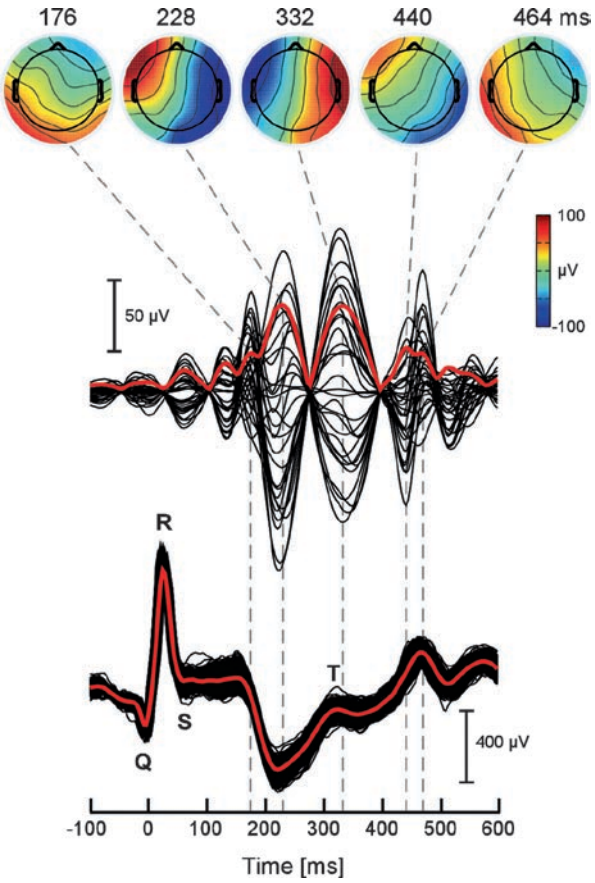

Fig. 2 Temporal characteristics of the pulse artefact, based on a typical 30-channel EEG recording in a 1.5 T MRI scanner. The *upper traces* show the evoked pulse artefact at all EEG channels. Overlaid in *red* is the mean global field power (GFP), which corresponds to the spatial standard deviation. Voltage maps are shown for selected GFP peak latencies. Note that, while some maps (176 and 464 ms; 228 and 440 ms) look similar, they are rotated differently, illustrating the temporal dynamics and spatial nonstationarity of the artefact. The distorted ECG is shown in the *bottom* part of the figure (see Fig. 1 for ECG recording details). Here, *black* traces refer to single cardiac cycles, with the Q wave used as the time-locking event and the *red* trace representing the average ECG. The T wave can be identified at about 300 ms, on top of the field-induced deflection at approximately 150-450 ms. The polarity of the ECG deflection depends on the orientation of the MRI B_0 field, and so it can be different at different MRI scanner sites

scanner type (head scanner, whole-body scanner), and the MRI B_0 field strength (1.5, 3 and 7 T). Therefore, the pulse artefact contributes a very dynamic - moving, rotating and polarity inverting - signal to the EEG, thus adding a range of topographies and signatures.

The lower part of Fig. 2 shows individual pulse artefacts and the averaged ECG, which shows that the ECG waveform is distorted by the influence of the magnetic field. Whereas

the QRS complex appears to be relatively unaffected, an additional deflection during the ejection phase of the cardiac cycle can be seen. An additional deflection can be observed between the onset of the S wave and the offset of the T wave (not present at 0 T). The latency range of this deflection roughly corresponds to the maximum artefact in the EEG, and can be substantially larger than the R wave (Debener et al. 2008). It is important to note, though, that the sign of this deflection depends on the polarity of the scanner's B_0 field, which varies between manufacturers.

Figures 1 and 2 illustrate the artefact in a case that is representative of commonly observed features: ECG-artefact delay and general topography, with its dynamic, rotational and polarity-inverting aspects.[3] The factors that can lead to differences in the artefact are linked to the subject and experimental setup. First of all, the theories for both of the postulated generative mechanisms, namely BCG and the Hall effect, predict that the artefact scales approximately proportionally with B_0 (Tenforde et al. 1983). This has been confirmed; the pulse artefact is much smaller at 1.5 T than at 3 and 7 T, with important consequences for the choice of artefact removal technique (Debener et al. 2008). Second, there are interindividual differences in patterns of cardiac activity, such as changes in heart rate, in peak latencies and morphology (Debener et al. 2008). Therefore, for those individuals with a higher heart rate (shorter interbeat interval), the pulse artefact activities between adjacent cardiac cycles may overlap to some extent, which could further complicate artefact removal (Vincent et al. 2007). Thirdly, the quality of the ECG recording may vary across subjects and/or sites, and it may not always be possible to identify the onset of every single cardiac cycle precisely. This can impair the performance of the pulse artefact removal procedures that rely on the detection of each cardiac cycle's onset. We conclude that the pulse artefact represents a rather complicated, dynamic contribution to the EEG. Thus, the development, application and comparison of pulse artefact removal procedures represents a real challenge.

3 Origin of the Pulse Artefact, Simulations and Modelling

The physical principles of electromagnetism state that any movement of electrically conductive material in a static magnetic field results in electromagnetic induction, and this is the fundamental cause of the pulse artefact. Therefore, motion related to cardiac activity can give rise to induced electromotive forces in the circuit formed by the EEG recording leads and subject, and be picked up by the EEG amplifier (see Fig. 3). However, the type of motion that is relevant to the pulse artefact is a matter of discussion. Some authors have suggested that axial head rotation is the primary cause (e.g. Nakamura et al. 2006), while others point to the possible local effect of pulsatile movements of scalp vessels on adjacent electrodes. In addition to ballistic effects, motion of the blood (i.e. abrupt changes in blood velocity) can lead to the Hall effect (a voltage difference is created on opposite sides of a

[3]For a movie illustration of the BCG time course and topography, the interested reader may wish to visit http://www.debener.de.

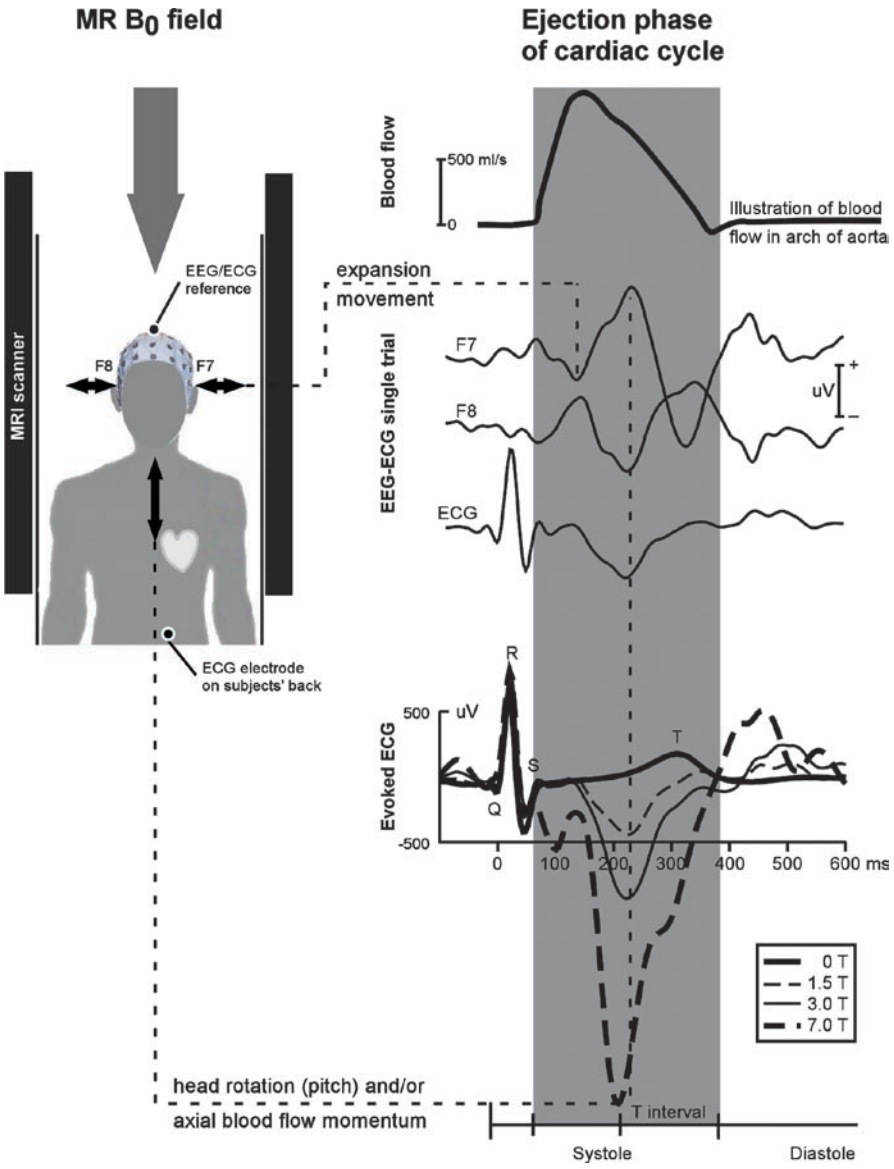

Fig. 3 A diagram illustrating factors that can cause the pulse artefact. Two different types of movement are indicated, axial nodding rotation of the head and expansion at lateral and temporal scalp sites. The *left* part of the figure illustrates a subject in the supine position inside an MRI scanner. The locations of the EEG electrodes, the EEG/ECG reference site and the ECG recording site on the lower back are indicated. The *lower right* part of the figure shows evoked ECG traces from one individual, recorded outside the MRI (0 T) and inside three different MRI scanners (1.5, 3.0, 7.0 T). A typical single trial of ECG and EEG activity is shown above the evoked ECG traces, and at the *top* , the time course of the blood fl ow in the arch of the aorta (as adapted from cardiac physiology textbooks) is shown. As highlighted by the *grey* background, the artefact mostly occurs during the ejection phase of the cardiac cycle. This figure is reprinted from Debener et al. 2008, with kind permission from Elsevier Publishers

moving conductor through which an electric current is flowing when placed in a strong magnetic field), which may also contribute to the pulse artefact.

In order to simulate the topographies of nodding head rotation and lateral electrode expansion, we recorded EEG data from a spherical phantom covered with a layer of conductive gel placed in a 1.5 T MRI scanner (see Fig. 4).[4] Lateral electrode expansion was simulated by inflating two balloons underneath the lateral electrodes, and axial head rotation was simulated by slightly rocking the whole phantom in the axial direction (i.e. in the direction of the B_0 field). Lateral electrode expansion lead to spatially circumscribed contributions, which could comprise positive, negative or biphasic deflections. The topographies resulting from axial and nodding head rotation closely resembled those observed in real subjects. Both basic, spatially unspecific map and polarity differences between the left and right hemisphere electrodes and polarity reversal (probably related to forwards–backwards motion) were evident in this simulation. Thus, this result clearly supports the role of nodding head rotation as a generator of the pulse artefact (Nakamura et al. 2006). However, the simulations did not reveal the rotational, moving aspect that is clearly present in real recordings. Accordingly, we conclude that rocking axial head rotation is the major, but not the only motion-related contribution to the pulse artefact.

Figure 3 summarizes multiple possible contributions to pulse artefact generation. The left hand part of the figure illustrates a subject in the supine position in the MRI scanner, along with the EEG and ECG electrode configuration usually used in our lab. The right hand part illustrates the typical time course of a cardiac cycle, with the blood flow illustration adapted from cardiac physiology textbooks. It can be seen that the onset of the pulse artefact roughly corresponds to the onset of the systole; that is, the onset of the blood ejection phase. During this period, the major pulse artefact deflections in both the EEG and ECG channels seem to occur. Note also the single-trial activities in channels F7 and F8 that are characterised by different polarities and also show the polarity reversal pattern over time. We speculate that the rotational aspect of the dynamic pulse artefact topography points towards a mixing of lateral electrode expansion and axial nodding head rotation. Unfortunately, at present, not enough is known about the temporal behaviour of these two processes, and the simulation study we reported above does not provide any insight into this matter. However, this type of information would be necessary in order to model topographies that could result from the interplay of lateral electrode expansion and axial nodding head rotation. Clearly, more studies are needed in order to isolate these potential pulse artefact contributions. This type of research could help to further our understanding of the pulse artefact, and thus help to achieve better EEG data quality from inside MRI scanner recordings.

Some authors recommended that an attempt should be made to reduce pulse artefacts prior to amplification by carefully laying out and immobilising the leads, twisting the leads, and using a bipolar electrode chain arrangement and a head vacuum cushion (Goldman et al 2000; Benar et al 2003). It is noteworthy that in EEG–fMRI studies in epilepsy, some investigators have found these measures to be sufficient, at least at 1.5 T, to analyse the EEG of epileptic patients. However, it is more common to combine these efforts with postprocessing artefact methods.

[4]These recordings were made at the Sir Peter Mansfield MRI Centre in Nottingham, UK. We are very grateful to Richard Bowtell and Karen Mullinger for sharing their ideas and our enthusiasm about EEG–fMRI and the pulse-related artefact.

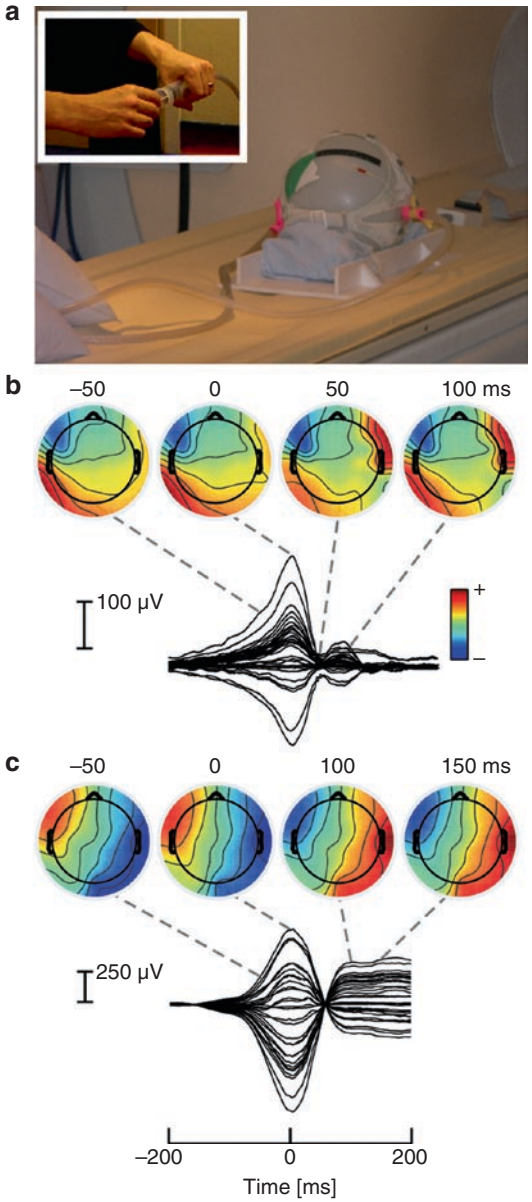

Fig. 4 Results of a motion simulation study. A spherical phantom was covered with a layer of electrode gel, fitted with an EEG cap, and positioned in the centre of an MRI scanner (**a**). Different types of motion were induced while EEG was recorded, among them bilateral expansion motion (**b**), as caused by the inflation of balloons positioned underneath temporal electrodes, and axial, nodding head motion (**c**). Recordings and the respective voltage topographies shown in (**b**) and (**c**) are based on averages over a few repetitions. Lateral expansion motion caused rather locally circumscribed voltages, which may resemble tangential (*left*) or radial (*right*) features. Axial nodding head rotation, on the other hand, contributed a low spatial frequency map, which was characterized by a polarity change over time, and by different polarities between left and right hemisphere electrodes

4 Reducing the Pulse Artefact Using Waveform Removal Approaches

In 1998, a seminal study on removing the pulse artefact was published (Allen et al. 1998). In this paper, Allen et al. introduced the average artefact subtraction (AAS) algorithm, which has become one of the most influential and frequently used methods. The algorithm

is predicated on the assumption that the EEG signals of interest (neuronal activity) and the ECG are not correlated, and that the artefact is relatively stable across a number of successive heartbeats. Therefore, in the ideal situation of a perfectly stable heartbeat, subtraction of the EEG averaged over a number of preceding heartbeats from the ongoing EEG will result in the removal of the artefact. While different implementations and developments of the AAS exist (Laufs et al. 2008), the basic principle of the AAS is common to all variants (see Fig. 5).

Figure 5 illustrates and highlights the main steps of the AAS method. First, the AAS approach requires knowledge of the precise onset of each cardiac cycle, which is usually obtained by simultaneously recording the ECG and detecting the onset of each cardiac cycle (e.g. all R peaks in the ECG). After this has been achieved, the next step is to define an artefact template. Importantly, this is done for each EEG channel separately and achieved by averaging the EEG over a predefined epoch preceding and time-locked to each cardiac cycle onset. The resulting artefact template represents the evoked pulse artefact with the ongoing EEG activity averaged out. The result is a moving average and subtraction procedure where the resulting template is subtracted from the current EEG epoch and thereby reduces the artefact. The procedure is repeated for every EEG channel and can be implemented in real time. In theory, the quality of the template increases with the number of epochs used. However, averaging more epochs reduces the sensitivity of the template to capture temporal fluctuations of the artefact. In spite of this limitation, many groups have found that the AAS procedure, which has been implemented in commercially

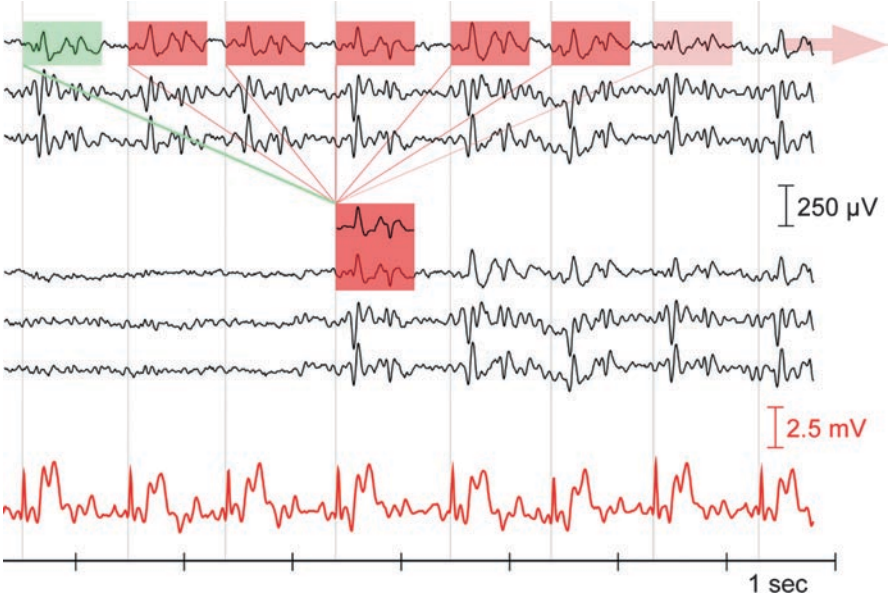

Fig. 5 Schematic of the average artefact subtraction procedure. For each channel, a waveform template is generated by averaging EEG epochs over adjacent cardiac cycles, with the time- locking event being derived from the ECG. The template generation is combined with a moving average procedure, and new templates are generated for each cardiac cycle. The procedure is repeated for each EEG channel

available and open source software packages, can give satisfactory EEG data quality (e.g. Hamandi et al. 2008; Sammer et al. 2005).

The limitations of the AAS algorithm result from deviations from the basic assumptions: a lack of correlation between stimulus (and response) and cardiac activity; temporal stability of the artefact; reliable and precise detection of the onset of each cardiac cycle. Any degree of correlation between cardiac activity and neuronal activity can be problematic from the point of view of EEG data quality, but the effects can be reduced by proper experimental design in evoked response studies (e.g. interstimulus interval jitter). Deviations from the stability assumption result in inaccurate artefact estimation and therefore lead to greater residual artefact after subtraction. Shortening the moving average window size cannot fully redress this problem, since a smaller moving average window would leave more residual EEG activity in the template.

The choice of template length is also potentially problematic due to variations in the R–R interval. Mismatch between template window length and artefact duration will lead to greater residual artefact. This has led to the introduction of alternative template generation schemes that either scale the pulse artefact template with a percentage of the mean R-R period in the moving average window (Ellingson et al. 2004) or that build a template which incorporates the pulse artefact data for all R-R period lengths present in the current moving average window (BrainVision Analyzer software). In the latter case, this template is then adaptively applied to each QRS period based on its R-R period, thus ensuring that no portion of the pulse artefact remains uncorrected due to a suboptimal template length.

Alternative template constructions that are based on weighted averages (Goldman et al. 2000) or median instead of mean values (Sijbers et al. 2000) have been devised. Also, some implementations allow for the selection of trials contributing to the template generation depending on whether they correlate sufficiently with other trials or not. This option helps to ensure that trials containing other EEG artefacts are excluded, thus improving the quality of the template used for subtraction. While all of these features may improve pulse artefact correction, they are not able to fully account for interartefact variability.

The cardiac cycle onset can be difficult to identify due to ECG channel contamination resulting from gradient switching and the effect of B_0 leading to missed cycles or inaccurate template estimation window alignment, and consequently degraded template estimates and residual artefacts. Accurate marker position improves the quality of the pulse artefact correction, in particular with regard to residual noise in the high-frequency range of the EEG signal. In our experience, efforts to ensure good ECG recording quality with a focus on a clear R wave through careful consideration of the positioning of electrodes are worthwhile. We usually derive the ECG from a single electrode attached to the lower back and referenced against the EEG reference (vertex or nearby) (e.g. Debener et al. 2005b, 2007, 2008). This scheme ensures large R peaks while avoiding respiratory and other movement-related artefacts on the ECG channel. While derivation schemes such as the classical Einthoven II ECG can yield clear R waves, they cannot easily be implemented inside the scanner, as they require long electrode leads that could also potentially pose a safety risk to the subjects. As a result, automatic R-wave detection algorithms developed for normal recording conditions may fail for intrascanner recordings and may provide inaccurate positioning of the event markers. One way to explore this further is to compute the standard deviation of the delays between the actual marker positions (e.g. Q wave) and the

following R wave latencies (Debener et al. 2008). Some implementations of the AAS algorithm, such as the BrainVision Analyzer (Brain Products GmbH, Munich, Germany), already take jitter information into account, and automatically align markers statistically such that the overall jitter is minimised before correction.

The problems inherent in the AAS approach have been investigated further by Niazy and colleagues (Niazy et al. 2005), and similarly by Negishi et al. (2004), who proposed a new way of constructing a pulse artefact template. These authors suggested generating pulse artefact templates based on a channel-wise temporal principal components analysis (PCA), thereby relaxing the stability requirement. Niazy and colleagues named this approach the optimal basis set (OBS) method, which refers to the first few principal components as representations of several distinct pulse artefact templates. These templates explain most of the artefact variance in any given EEG channel and are jointly used to regress the pulse artefact from the EEG data. The OBS approach therefore tries to account for greater temporal variation in the artefact shape. The resulting software tool is a freely available Matlab plug-in that interacts with the open-source EEGLAB environment (Delorme and Makeig 2004). A potential limitation of this approach is that the number of necessary artefact templates are not indicated by the software and need to be determined by the user.

Other channel-by-channel correction approaches exist that account for the template duration problem. For instance, Bonmassar et al. utilized an adaptive Kalman filter approach (Bonmassar et al. 2002), which requires an extra motion sensor signal to be recorded as a reference signal. However, it might be feasible to use electrooculogram (EOG) signals instead (In et al. 2006). A novel method for recording motion has been proposed by Masterton et al. (2007), who attached three loops as motion sensors on an electrode cap. This group reported a more complete model of head movements and, when employing a linear adaptive filter technique, good correction of the pulse-related artefact and (other) head movement artefacts. While apparently producing good corrections, the Kalman filter approach appears to be computationally demanding, and is based on the questionable assumption that the EEG signal has a white noise characteristic (In et al. 2006). Other methods such as a wavelet-based nonlinear reduction of the pulse artefact (Wan et al. 2006) are also computationally demanding and are therefore unlikely to supplant AAS in the near future. Recently, Vincent and colleagues (Vincent et al. 2007) proposed a moving general linear model approach (mGLM), along with evidence of improved performance compared to the AAS. These authors address the specific issue of pulse artefact that lasts longer than a cardiac cycle. It remains to be determined whether this is indeed a significant problem, and whether the mGLM approach provides a major improvement over the AAS.

5 Removing the Pulse Artefact Using Spatial Pattern Removal Approaches

The abovementioned AAS, OBS and mGLM approaches all aim to model the pulse artefact waveform. This is usually done for each EEG channel separately, taking into account the fact that different channels show different artefact morphologies. However, as already shown in Fig. 2, the pulse artefact can be also characterised by a number of typical topog-

raphies, which may be sufficiently different from topographies of neuronal origin to be identifiable. The potential virtue of spatial approaches, which aim to remove those topographies, is that exact knowledge of the onset of each cardiac cycle is not necessarily required. Thus, in principle, a spatial approach can avoid problems that are inherent to AAS and OBS, as discussed above.

Motivated by the success of spatial approaches for the removal of EEG eye blink and eye movement artefacts, two spatial pulse artefact correction approaches have been proposed (Benar et al. 2003): PCA and independent component analysis (ICA). The assumption behind these is that the pulse artefact contribution is physiologically independent from, or in the case of PCA orthogonal to, ongoing EEG activity. Therefore, pulse artefact activity is presumed to be contained in a small number of components, whereas all other EEG activity should be represented by the remaining components. In the original work by Benar and colleagues, pulse artefact components were visually identified by exploring the similarity of all component time courses to the simultaneously recorded ECG signal (Benar et al. 2003). Back-projection of remaining components resulted in reconstructed EEG traces with reduced artefact. Benar and colleagues found that both ICA and PCA were well suited for this task, as they eliminated pulse artefact activity while preserving the relative amplitudes of epileptic spikes.

However, the subjective selection of components is a limitation of this approach, since it makes its performance user dependent and requires training. Indeed, it can be rather difficult to visually identify and select the components that represent pulse artefact activity beyond the first few strongest and most obvious ones. Srivastava et al. (2005) proposed the identification of independent components based on their degree of correlation with the ECG. A comparison of a fully automatic implementation of ICA, OBS and OBS-ICA methods found that the latter two provided superior performance (Debener et al. 2007). Possible explanations for the difference are as follows. First, the selection-by-correlation approach does not identify the correct components (that is, those reflecting the pulse artefact) because the independent components represent a linear decomposition of the EEG artefact rather than the electrical ECG signal. Second, it may be that ICA is not able to disentangle ongoing and event-related EEG activity from pulse artefact activity due to violations of the spatial stationarity assumption that underlies temporal ICA. With regard to the first concern, an alternative approach for component identification can be used, as shown in Fig. 6. Here, the components were identified by the amount of variance they contributed to the evoked pulse artefact, rather than based on the degree of correlation with the ECG. As illustrated, five components explained nearly all of the pulse artefact variance in this particular dataset (30-channel EEG recorded at 1.5 T). When compared to the identification-by-correlation criterion, we found evidence that this latter approach gives better results (Debener et al. 2008).

While several groups have reported success in using ICA for pulse artefact removal (e.g. Benar et al. 2003; Briselli et al. 2006; Eichele et al. 2005; Huiskamp 2005; Mantini et al. 2007; Nakamura et al. 2006), some results have been less positive (Debener et al.2007, 2008). A possible reason for this discrepancy is the field strength of the scanners used in these studies. A study using resting-state EEG data from the one individual was performed at 1.5, 3 and 7 T and the results were compared to recordings made at 0 T.

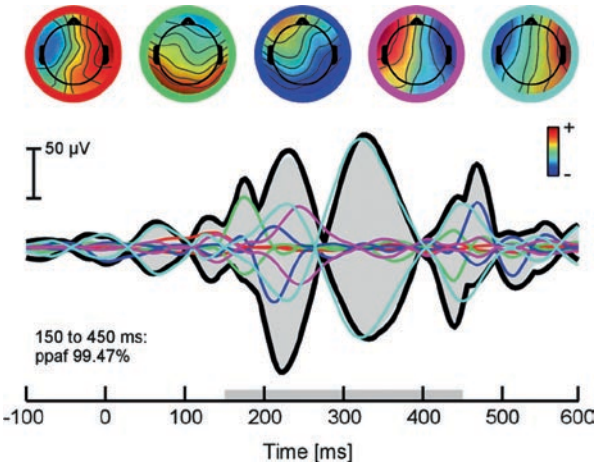

Fig. 6 Typical example of the use of ICA to remove the pulse artefact. Using the EEGLAB function "envtopo", the independent components that explain most of the variance of an evoked signal in a specified time range (here 150–450 ms) can be identified. In this case, five components were selected and accounted for >99% of the variance of the evoked signal. Shown are the envelope of the sensor data (*black*), which reflects the minima and maxima across all channels, and the envelope of the joint back-projection of the five independent components (*grey shaded area*). For each component, the map (i.e. inverse weights) and the envelope of the back-projection (coloured traces) are shown. *ppaf*, percentage of power accounted for

At 1.5 T, the ICA decomposition was found to be comparable to that obtained from data recorded outside the MRI, while the decompositions for data recorded at 3 and 7 T were markedly different. These findings are consistent with field-strength-dependent violations of the ICA assumptions. For example, the spatial stationarity assumption may be violated by the pulse artefact amplitude and spatial variability, which increases at higher fields, possibly reflecting the moving, rotating patterns previously described. As a result, ICA requires more components to model the pulse artefact at higher field strengths, and may be incompatible with the assumption of one (or a few) fixed sources (Nakamura et al. 2006). Further analyses of EEG and ECG are consistent with the notion that two different processes give rise to the BCG: blood movement or axial head rotation and electrode movement on the sides of the head. A BCG model has been proposed which may help to explain some of the observed inconsistencies in the usefulness of ICA for BCG removal (Debener et al. 2008).

In summary, the available evidence suggests that the spatial filtering approaches such as ICA and PCA may not be as efficient when used as template methods, particularly at fields of 3 T and higher. The application of ICA in combination with ECG-triggered template subtraction methods such as AAS and OBS offers a possible way forward.

Kim and coworkers combined a wavelet-based denoising approach with recursive adaptive filtering as postprocessing only in cases where AAS failed (Kim et al. 2004). Likewise, Niazy et al. (2005) suggest the use of adaptive noise cancellation following OBS

to increase performance. A comparison of ICA with the identification-by-correlation approach (Srivastava et al. 2005), OBS (Niazy et al. 2005), and a combination of both (Debener et al. 2005b) showed that ICA, when used on its own, while reducing the pulse artefact substantially, also reduced the signal-to-noise ratios (SNRs) of ERPs. This suggests that artefact and signal could not be disentangled very well by ICA. However, when used after OBS, infomax ICA improved the ERP SNR and the ERP topography. Moreover, this combination can be used to remove eye blinks, and to identify brain-related signals (Debener et al. 2005a, b, 2006).

6 Evaluation of Pulse Artefact Removal Approaches

There is a lack of consistency in the evaluation of EEG artefact removal methods. There is a tendency to focus on the reduction of the pulse artefact removed from the signal. However, this approach does not necessarily address the issue of signal preservation. In the extreme case, all of the signal could be suppressed, including the undesirable artefact. Depending on the application, it may be best to avoid the use of a particular artefact correction method. Therefore, performance evaluation schemes must also address the correction algorithm's specificity—its capacity to preserve genuine neuronal signals. It is therefore a better strategy to quantify the amount of pulse artefact correction *and* the preservation of the aspect of the EEG that is of interest (epileptic spike, ERP, brain rhythm, spectrogram). If possible, the signal measured inside the scanner should be compared to an equivalent dataset recorded outside the scanner (≈ 0 T). For example, in studies designed to evaluate the performance of a correction method to be applied to event-related potential recordings, it is important to measure the SNR of the ERP component of interest and its topography (Handy 2005). The topographic quality of the corrected ERPs could be quantified by calculating the deviation to a reference recording topography or source reconstruction (Debener et al. 2007, 2008). Also, measures of the recovery of the EEG spectrum can be included, particularly if the EEG variable of interest is in the frequency or time-frequency domain (e.g. Allen et al. 1998). Moreover, hybrid simulation studies may be very informative when evaluating EEG signal quality. In any case, a better understanding of the mechanisms that give rise to the cardiac-related artefacts should lead to improved artefact reduction and expand the scope for the application of EEG–fMRI.

7 Conclusions

The pulse artefact is readily visible in EEGs recorded inside MR scanners and is generally larger at higher field strengths. It can interfere with the identification of events of interest, from large spikes in the recordings from epileptic patients to EEG oscillations and

low-amplitude ERPs. While it is possible to reduce its magnitude at the source, this is unlikely to be sufficient for most applications, and particularly in the field of ERP. Different methods have been proposed for removing the pulse artefact, and an increasing number of publications that aim to tackle this issue are being published, which is encouraging and will help to further improve the EEG signal quality that can be achieved. Further progress in this field could be achieved with a more detailed knowledge of the precise origin of the pulse artefact. Nevertheless, when used correctly, existing methods such as AAS and OBS can, depending on the application, provide EEG data of sufficient quality. We have highlighted divergent views on the virtues of spatial filter tools such as ICA for pulse artefact removal. Data-driven methods such as ICA, when used in combination with AAS or OBS, appear capable of further reducing residual artefacts, and may play an increasingly important role in the integration of EEG and fMRI beyond mere artefact removal. Finally, the field would benefit from standardised artefact reduction evaluation procedures and methods that are capable of providing absolute performance measures and therefore facilitate comparisons.

References

Allen PJ, Polizzi G, Krakow K, Fish DR, Lemieux L (1998) Identification of EEG events in the MR scanner: the problem of pulse artefact and a method for its subtraction. Neuroimage 8(3): 229–239

Babiloni F, Mattia D, Babiloni C, Astolfi L, Salinari S, Basilisco A, Rossini PM, Marciani MG, Cincotti F (2004) Multimodal integration of EEG, MEG and fMRI data for the solution of the neuroimage puzzle. Magn Reson Imaging 22(10):1471–1476

Benar CG, Aghakhani Y, Wang YH, Izenberg A, Al-Asmi A, Dubeau F, Gotman J (2003) Quality of EEG in simultaneous EEG–fMRI for epilepsy. Clin Neurophysiol 114(3):569–580

Bonmassar G, Purdon PL, Jaaskelainen IP, Chiappa K, Solo V, Brown EN, Belliveau JW (2002) Motion and ballistocardiogram artefact removal for interleaved recording of EEG and EPs during MRI. Neuroimage 16(4):1127–1141

Briselli E, Garreffa G, Bianchi L, Bianciardi M, Macaluso E, Abbafati M, Grazia Marciani M, Maraviglia B (2006) An independent component analysis-based approach on ballistocardiogram artefact removing. Magn Reson Imaging 24(4):393–400

Debener S, Makeig S, Delorme A, Engel AK (2005a) What is novel in the novelty oddball paradigm? Functional significance of the novelty P3 event-related potential as revealed by independent component analysis. Cogn Brain Res 22(3):309–321

Debener S, Mullinger KJ, Niazy RK, Bowtell RW (2008) Properties of the ballistocardiogram artefact as revealed by EEG recordings at 1.5, 3 and 7 T static magnetic field strength. Int J Psychophysiol 67(3):189–199

Debener S, Strobel A, Sorger B, Peters J, Kranczioch C, Engel AK, Goebel R (2007) Improved quality of auditory event-related potentials recorded simultaneously with 3-T fMRI: Removal of the ballistocardiogram artefact. Neuroimage 34(2):590–600

Debener S, Ullsperger M, Siegel M, Engel AK (2006) Single-trial EEG/fMRI reveals the dynamics of cognitive function. Trends Cogn Sci 10(12):558–563

Debener S, Ullsperger M, Siegel M, Fiehler K, von Cramon DY, Engel AK (2005b) Trial-by-trial coupling of concurrent electroencephalogram and functional magnetic resonance imaging identifies the dynamics of performance monitoring. J Neurosci 25(50):11730–11737

Delorme A, Makeig S (2004) EEGLAB: An open source toolbox for analysis of single-trial EEG dynamics including independent component analysis. J Neurosci Methods 134(1):9–21
Eichele T, Specht K, Moosmann M, Jongsma ML, Quiroga RQ, Nordby Hand Hugdahl K (2005) Assessing the spatiotemporal evolution of neuronal activation with single-trial event-related potentials and functional MRI. Proc Natl Acad Sci USA 102(49):17798–17803
Ellingson ML, Liebenthal E, Spanaki MV, Prieto TE, Binder JR, Ropella KM (2004) Ballistocardiogram artefact reduction in the simultaneous acquisition of auditory ERPS and fMRI. Neuroimage 22(4):1534–1542
Goldman RI, Stern JM, Engel J, Cohen MS (2000) Acquiring simultaneous EEG and functional MRI. Clin Neurophysiol 111(11):1974–1980
Hamandi K, Laufs H, Nöth U, Carmichael DW, Duncan JS, Lemieux L (2008) BOLD and perfusion changes during epileptic generalised spike wave activity. Neuroimage 39(2):608–618
Handy TC (2005) Event-related potentials: a methods handbook. The MIT Press, Cambridge
Herrmann CS, Debener S (2007) Simultaneous recording of EEG and BOLD responses: a historical perspective. Int J Psychophysiol 67(3):161–168
Horwitz B, Poeppel D (2002) How can EEG/MEG and fMRI/PET data be combined? Hum Brain Mapp 17(1):1–3
Huiskamp, G.J. (2005). Reduction of the Ballistocardiogram Artifact in Simultaneous EEG-fMRI using ICA. Conf Proc IEEE Eng Med Biol Soc, 4, 3691–3694
In, M.H., Lee, S.Y., Park, T.S., Kim, T.S., Cho, M.H., & Ahn, Y.B. (2006). Ballistocardiogram artifact removal from EEG signals using adaptive filtering of EOG signals. Physiological Measurement, 27, 1227–1240
Kim KH, Yoon HW, Park HW (2004) Improved ballistocardiac artefact removal from the electroencephalogram recorded in fMRI. J Neurosci Methods 135(1–2):193–203
Laufs H, Daunizeau J, Carmichael DW, Kleinschmidt A (2008) Recent advances in recording electrophysiological data simultaneously with magnetic resonance imaging. Neuroimage 40(2): 515–528
Mantini D, Perrucci MG, Cugini S, Ferretti A, Romani GL, Del Gratta C (2007) Complete artefact removal for EEG recorded during continuous fMRI using independent component analysis. Neuroimage 34(2):598–607
Masterton, R.A., Abbott, D.F., Fleming, S.W., & Jackson, G.D. (2007). Measurement and reduction of motion and ballistocardiogram artefacts from simultaneous EEG and fMRI recordings. Neuroimage, 37, 202–211
Nakamura W, Anami K, Mori T, Saitoh O, Cichocki A, Amari S (2006) Removal of ballistocardiogram artefacts from simultaneously recorded EEG and fMRI data using independent component analysis. IEEE Trans Biomed Eng 53(7):1294–1308
Negishi M, Abildgaard M, Nixon T, Constable RT (2004) Removal of time-varying gradient artefacts from EEG data acquired during continuous fMRI. Clin Neurophysiol 115(9):2181–2192
Niazy RK, Beckmann CF, Iannetti GD, Brady JM, Smith SM (2005) Removal of FMRI environment artefacts from EEG data using optimal basis sets. Neuroimage 28(3):720–737
Parkes LM, Bastiaansen MC, Norris DG (2006) Combining EEG and fMRI to investigate the post-movement beta rebound. Neuroimage 29(3):685–696
Sammer G, Blecker C, Gebhardt H, Kirsch P, Stark R, Vaitl D (2005) Acquisition of typical EEG waveforms during fMRI: SSVEP, LRP, and frontal theta. Neuroimage 24(4):1012–1024
Sijbers J, Van Audekerke J, Verhoye M, Van der Linden A, Van Dyck D (2000) Reduction of ECG and gradient related artefacts in simultaneously recorded human EEG/MRI data. Magn Reson Imaging 18(7):881–886
Skrandies W (1990) Global field power and topographic similarity. Brain Topogr 3(1):137–141
Srivastava G, Crottaz-Herbette S, Lau KM, Glover GH, Menon V (2005) ICA-based procedures for removing ballistocardiogram artefacts from EEG data acquired in the MRI scanner. Neuroimage 24(1):50–60

Tenforde TS, Gaffey CT, Moyer BR, Budinger TF (1983) Cardiovascular alterations in *Macaca* monkeys exposed to stationary magnetic fields: experimental observations and theoretical analysis. Bioelectromagnetics 4(1):1–9

Vincent JL, Larson-Prior LJ, Zempel JM, Snyder AZ (2007) Moving GLM ballistocardiogram artefact reduction for EEG acquired simultaneously with fMRI. Clin Neurophysiol 118(5): 981–998

Wan X, Iwata K, Riera J, Ozaki T, Kitamura M, Kawashima R (2006) Artefact reduction for EEG/fMRI recording: Nonlinear reduction of ballistocardiogram artefacts. Clin Neurophysiol 117(3):668–680